Supporting Information for

Sequential supramolecular assembly of tannic acid and phenylboronic acid copolymers enabling enhanced cancer immunotherapy

Anudari Batbayar [a,b], Ryotaro Ohashi [a,b], Yuto Honda [*a,b,c], Haochen Guo [c], Makoto Matsui [b], Takahiro Nomoto [a,d], Yutaka Miura [a,b] and Nobuhiro Nishiyama [*a,b,c]

[a] Laboratory for Chemistry and Life Science, Institute of Integrated Research, Institute of Science Tokyo, 4259 Nagatsuta-cho, Midori-ku, Yokohama, Kanagawa, 226-8501, Japan.

[b] Department of Life Science and Technology, School of Life Science and Technology, Institute of Science Tokyo, 4259 Nagatsuta-cho, Midori-ku, Yokohama, Kanagawa, 226-8501, Japan.

[c] Innovation Center of Nanomedicine (iCONM), Kawasaki Institute of Industrial Promotion, 3-25-14 Tonomachi, Kawasaki-ku, Kawasaki, Kanagawa, 210-0821, Japan.

[d] Department of Life Sciences, Graduate School of Arts and Sciences, The University of Tokyo, 3-8-1 Komaba, Meguro-ku, Tokyo 153-8902, Japan.

*Correspondence should be addressed: honda.y.aj@m.titech.ac.jp (Y. H.), nishiyama.n.ad@m.titech.ac.jp (N. N.)

Supplementary Scheme:

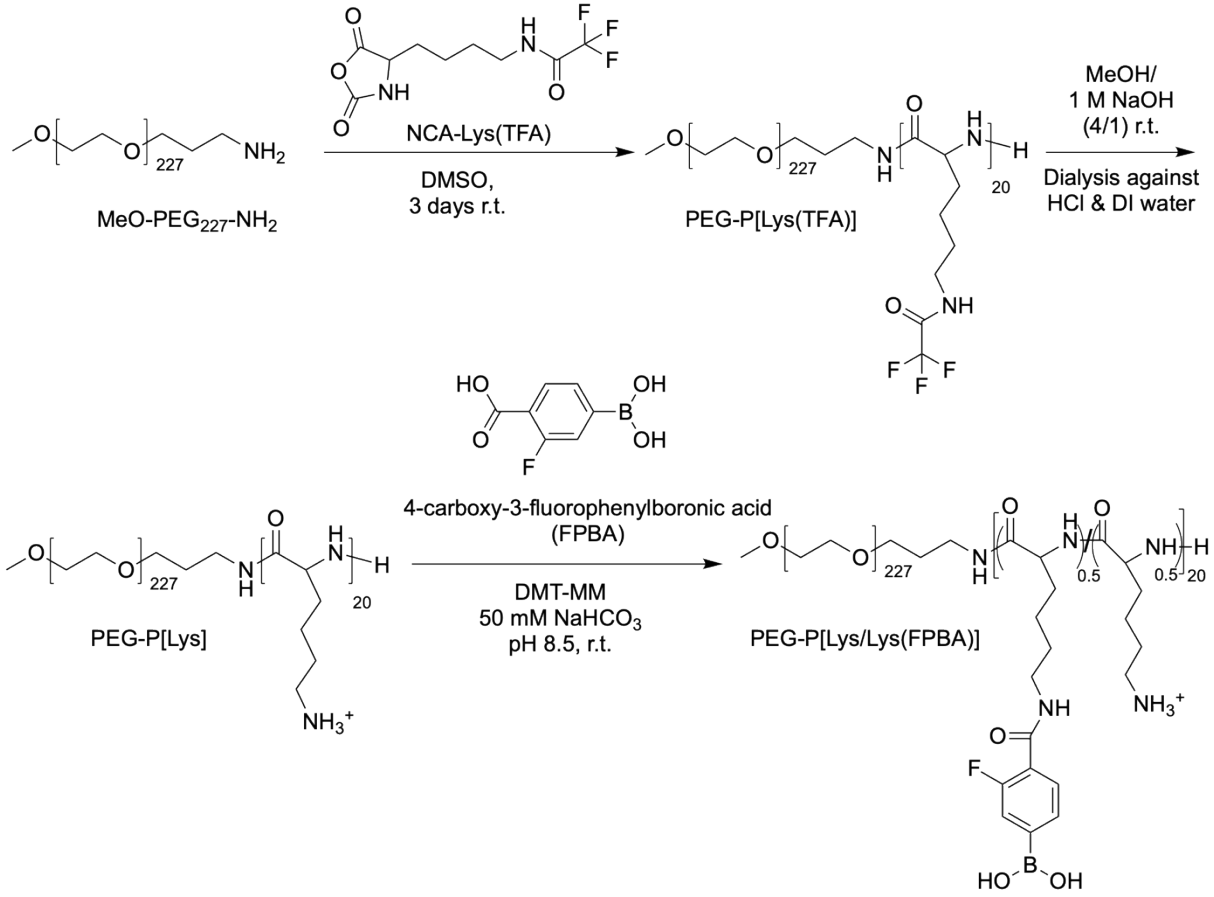

Scheme S1. Synthetic scheme for PEG-PLys(FPBA)

Supplementary Figures:

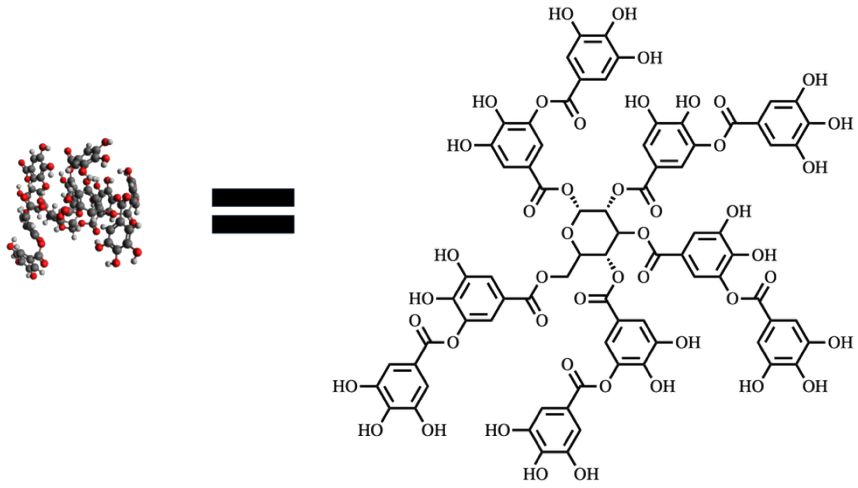

Figure S1. Representative chemical structure of tannic acids (TA)

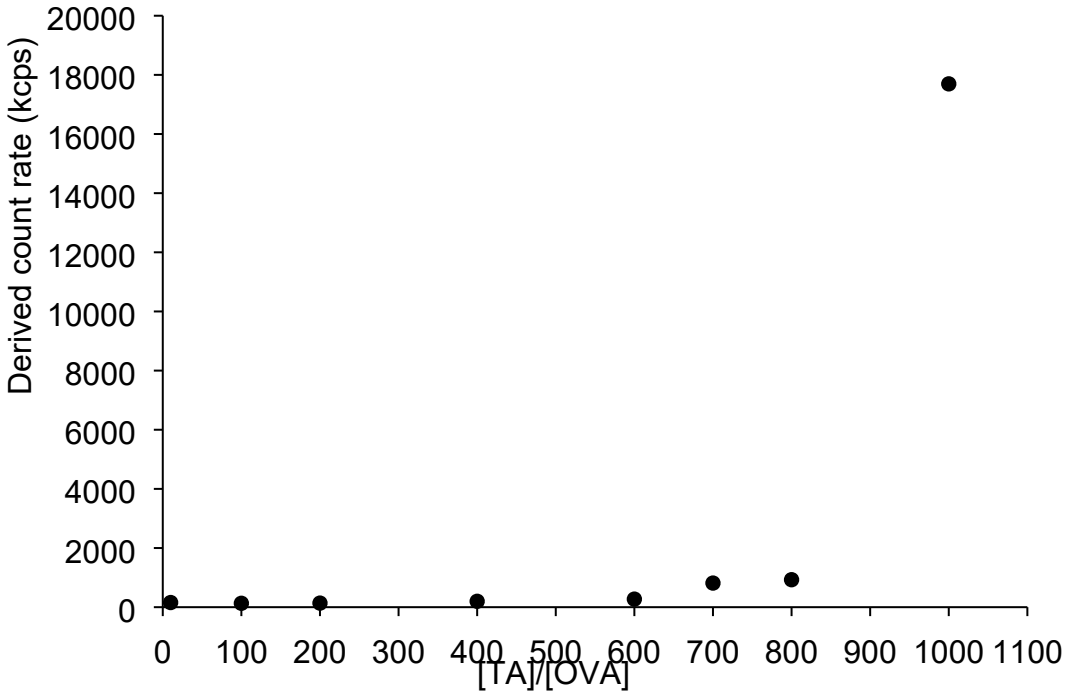

Figure S2. Turbidity measurement by light scattering analysis. OVA concentration, 1.0 mg mL^{-1} (1.1 μM).

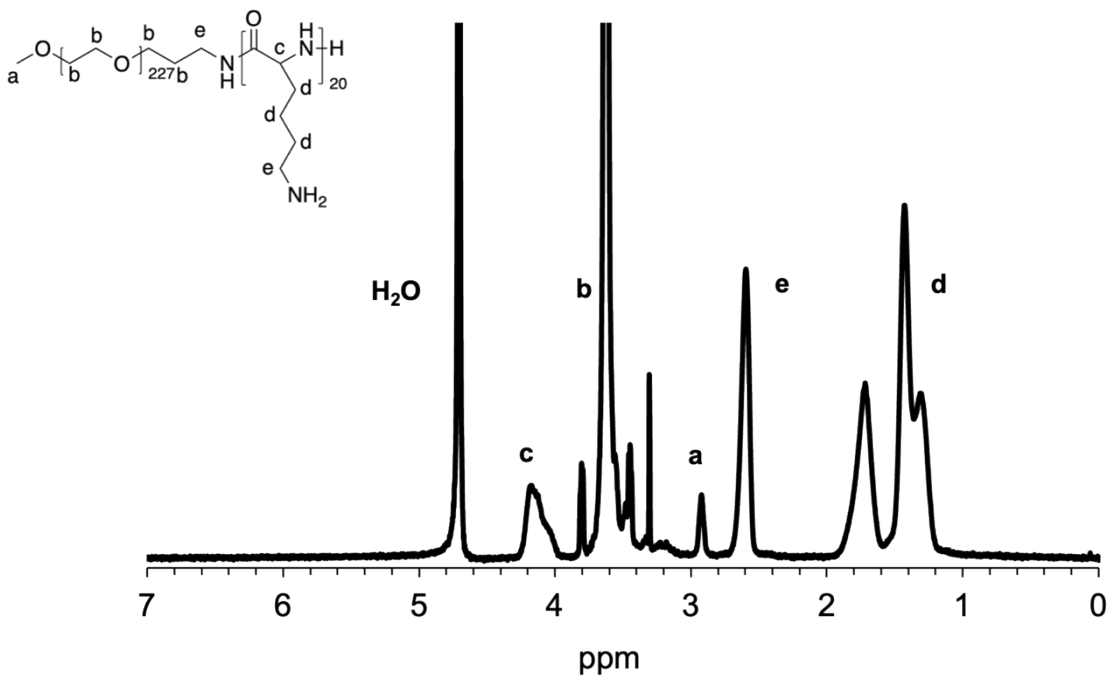

Figure S3. ^{1}H NMR spectrum of PEG-PLys (solvent: D_2O).

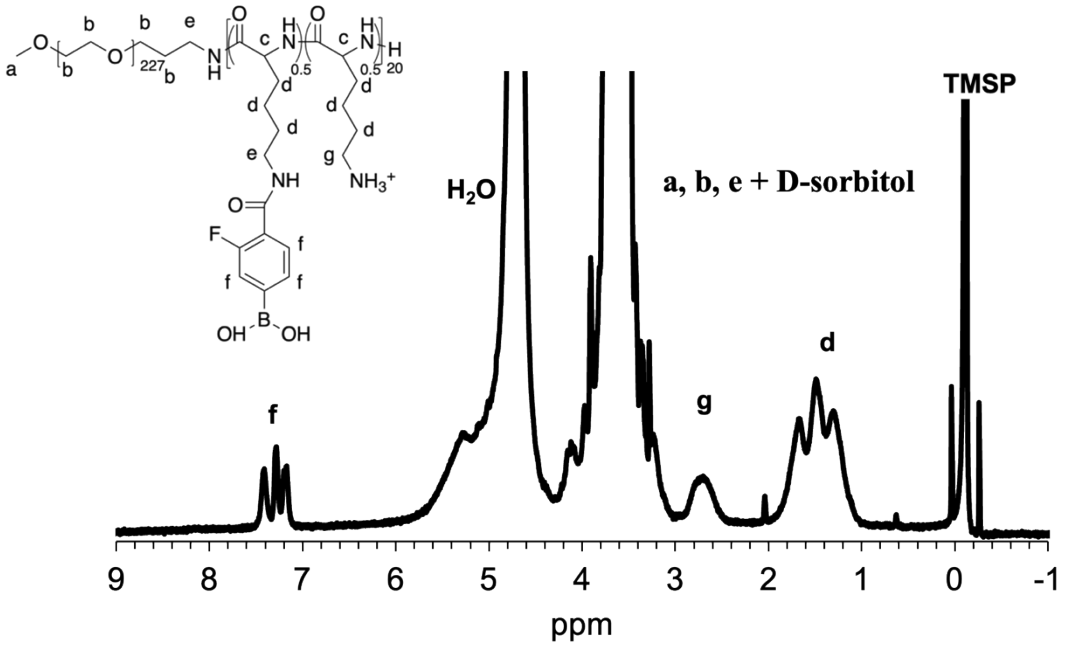

Figure S4. ^{1}H NMR spectrum of PEG-PLys(FPBA) (solvent: D_2O with 5% NaODaq and 20 mg mL^{-1} of D-sorbitol).

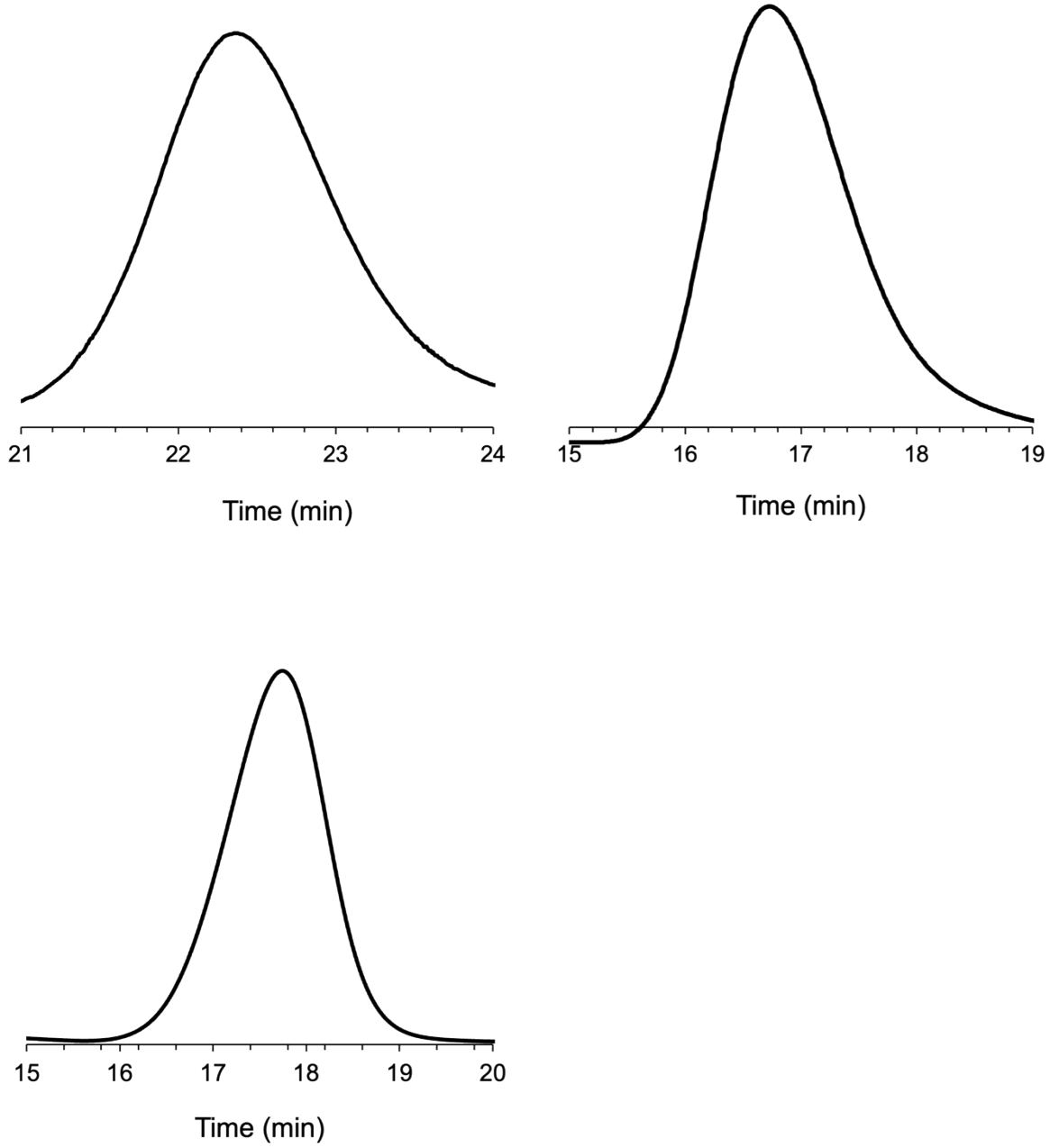

Figure S5. GPC charts. (a) PEG-PLys(TFA) (column: TSKgel superAW3000 and superAW4000, Eluent: NMP containing 50 mM LiBr, Flow rate: 0.2 mL min^{-1}, 40°C, calibrated against PEG standards. (b) PEG-PLys (column: Superdex 200 Increase 10/300 GL, Eluent: 10 mM HEPES with 150 mM NaCl, Flow rate: 0.75 mL min^{-1}, room temperature. (c) PEG-PLys(FPBA) (column: Superdex 200 Increase 10/300 GL, Eluent: 10 mM HEPES with 150 mM NaCl, 500 mM D-sorbitol, Flow rate: 0.75 mL min^{-1}, room temperature.

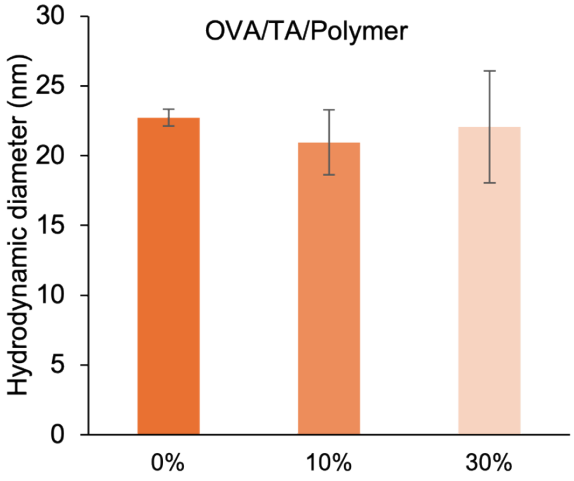

Figure S6. Serum stability of OVA ternary complex. The hydrodynamic diameter was measured by FCS in D-PBS(-) containing FBS with 0, 10, and 30 vol%. Data are presented as mean ± SD (n = 10).

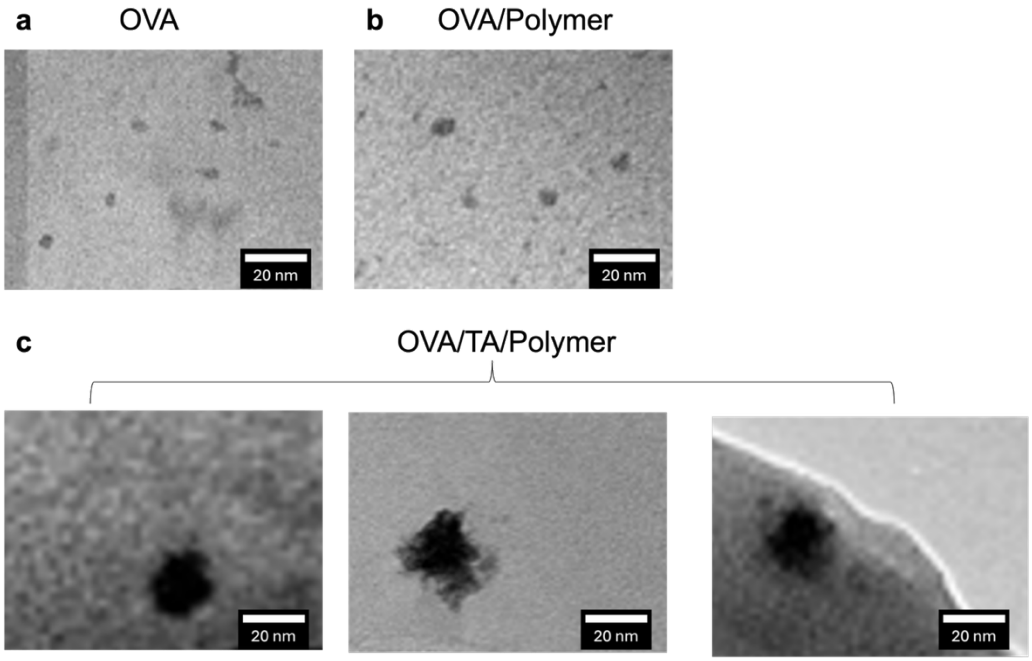

Figure S7. Representative TEM images of (a) OVA, (b) OVA/Polymer, and (c) OVA/TA/Polymer ternary complex. Scale bar: 20 nm.

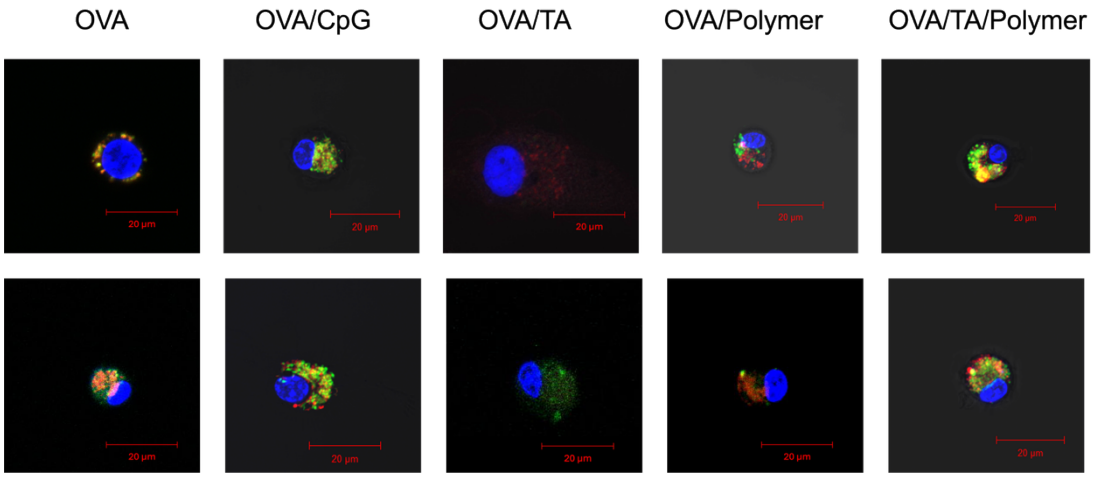

Figure S8. Additional CLSM images of BMDCs following incubation with each treatment group. Blue: nuclei (Hoechst 33342); Green: OVA; Red: late endosomes/lysosomes (LysoTracker Red). Scale bar = 20 μm.

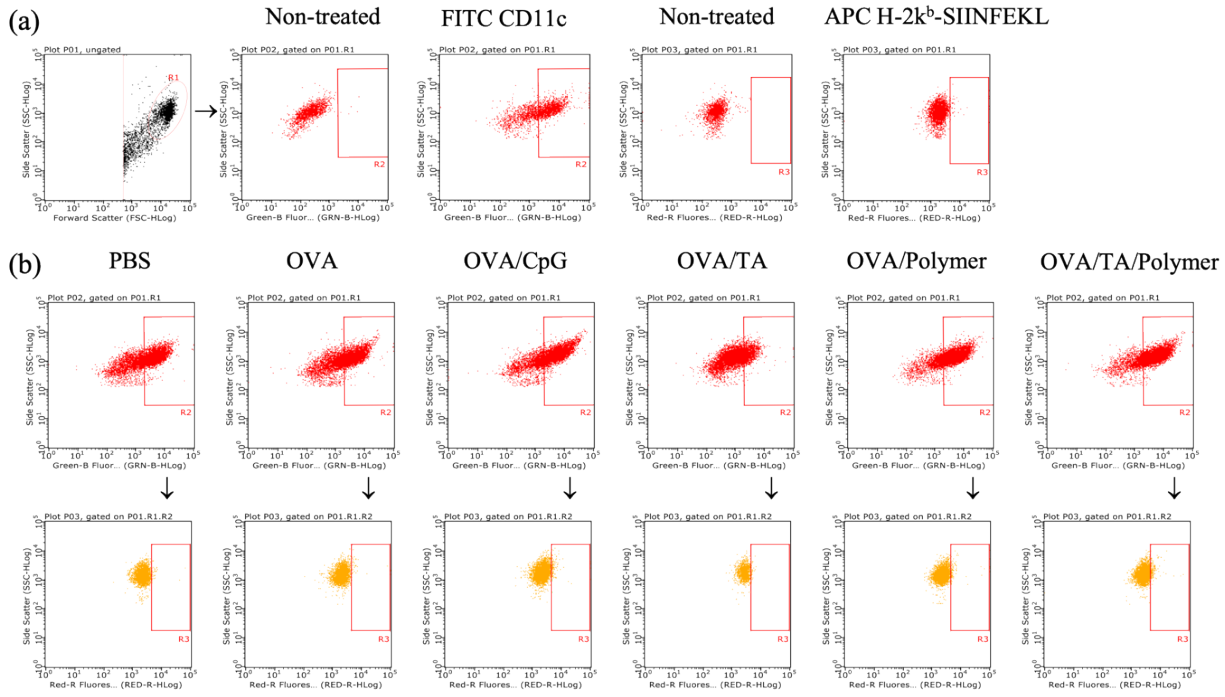

Figure S9. *In vitro* analysis of H-2k^b-SIINFEKL$^+$ CD11c$^+$ BMDCs following 24 hours incubation with OVA samples. (a) Gating strategy. (b) Representative plots showing H-2k^b-SIINFEKL$^+$ CD11c$^+$ cell populations in BMDCs in each sample.

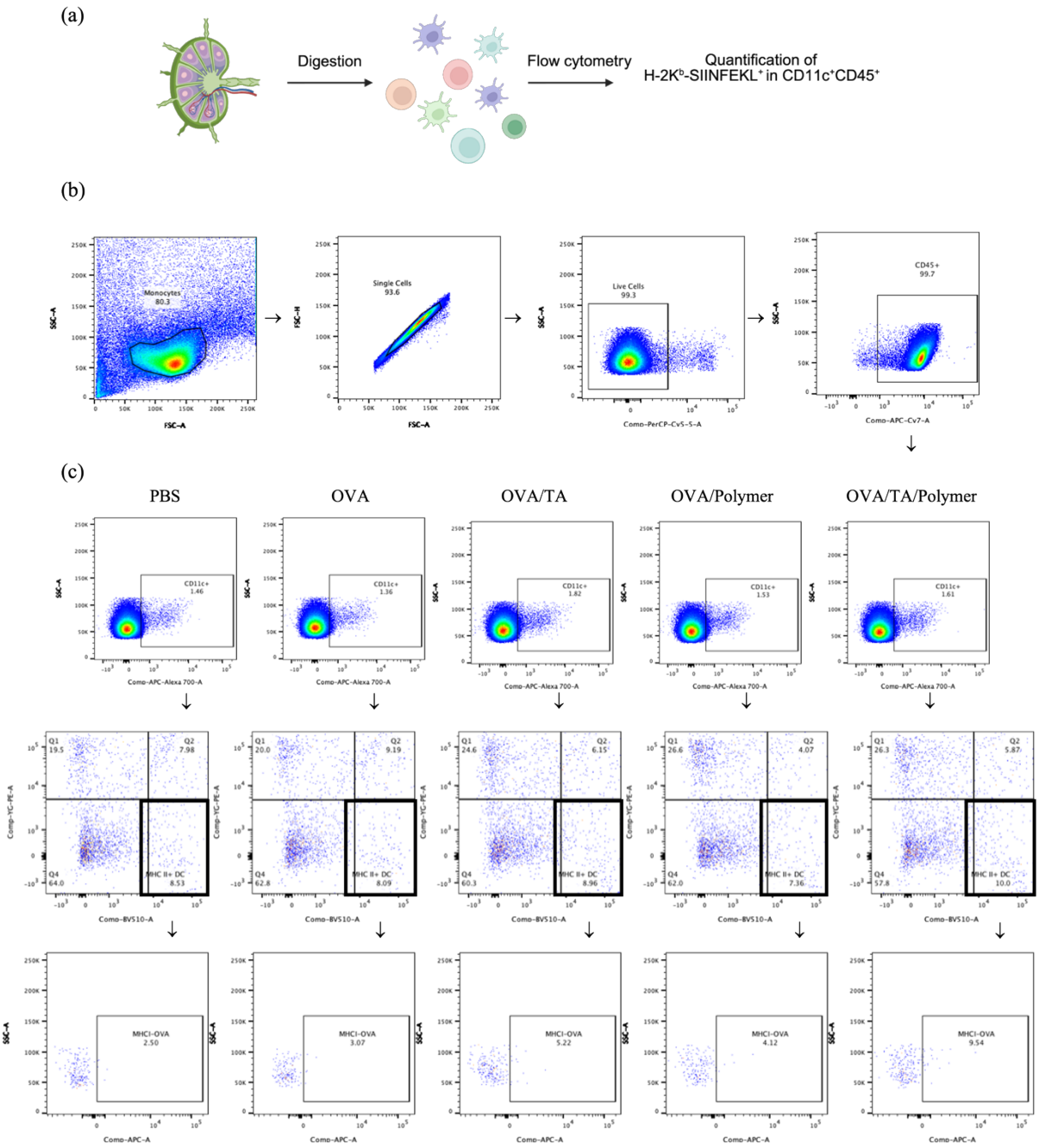

Figure S10. *In vivo* gating strategy for H-2k^{b}-SIINFEKL^{+} CD11c^{+} DCs in iLNs. OVA samples were injected s.c. on days 0 and 7**.** On day 14, iLNs were harvested for analysis. (a) Antigen-presentation study design. (b) Gating strategy for CD45^{+} cells. (c) Representative plots of H-2k^{b}-SIINFEKL^{+} CD11c^{+} DCs from CD45^{+} cells.

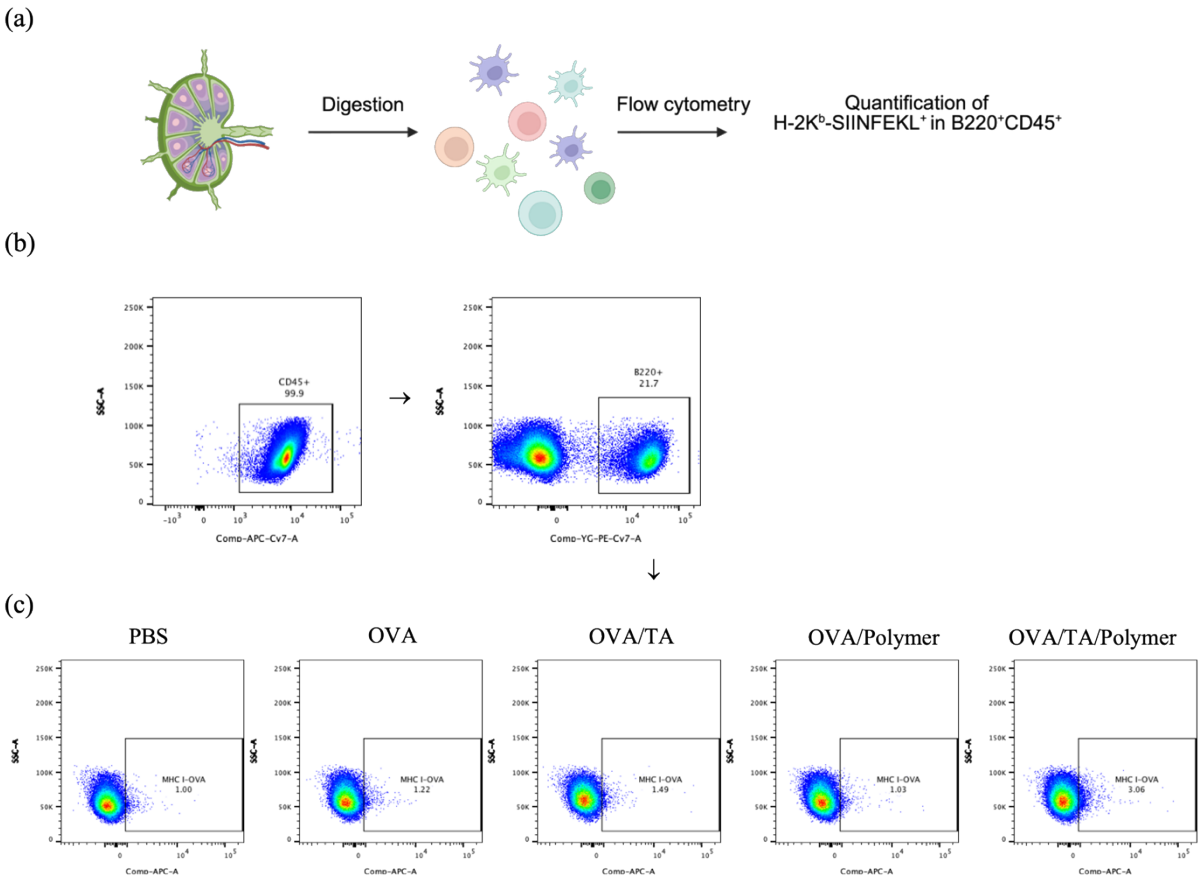

Figure S11. ***In vivo*** **gating strategy for H-2k^b-SIINFEKL$^+$ B220$^+$ antigen presenting B cells in iLNs.** OVA samples were injected s.c. on days 0 and 7**.** On day 14, iLNs were harvested for analysis. (a) Antigen-presentation study design. (b) Gating strategy for CD45$^+$ cells. (c) Representative plots of H-2k^b-SIINFEKL$^+$ B220$^+$ B cells from CD45$^+$ cells.

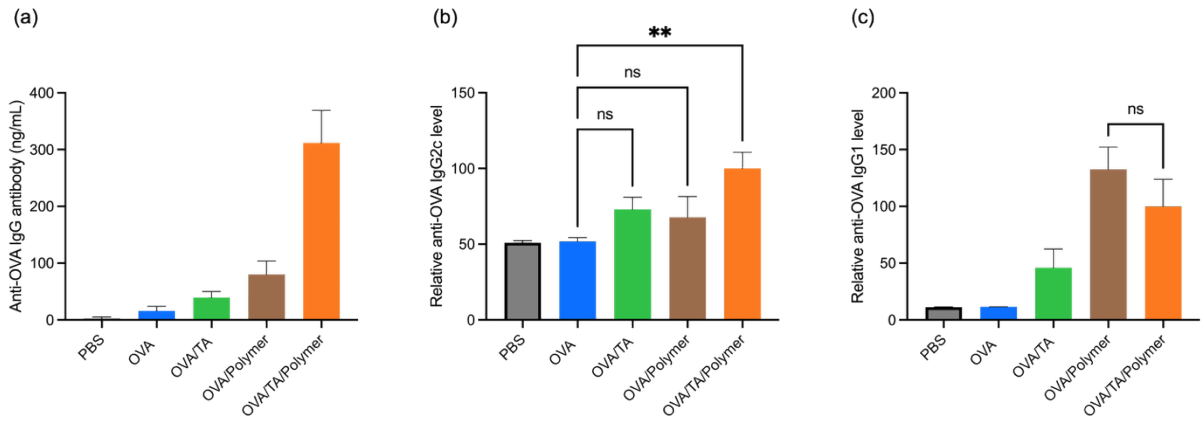

Figure S12. Serum anti-OVA antibody levels in each treatment group. OVA samples were injected s.c. on days 0 and 7**.** On day 14, whole blood was collected, serum was isolated and antibody levels were quantified by ELISA (OVA: 10 µg per mouse; n = 4 mice). Serum anti-OVA (a) IgG concentration (ng mL^{-1}). Relative serum anti-OVA (b) IgG2c and (c) IgG1 antibody levels were normalized to the OVA/TA/Polymer group (set to 100). The results are expressed as mean ± SEM. Statistical significance was determined by ANOVA with Tukey's multiple comparison test.

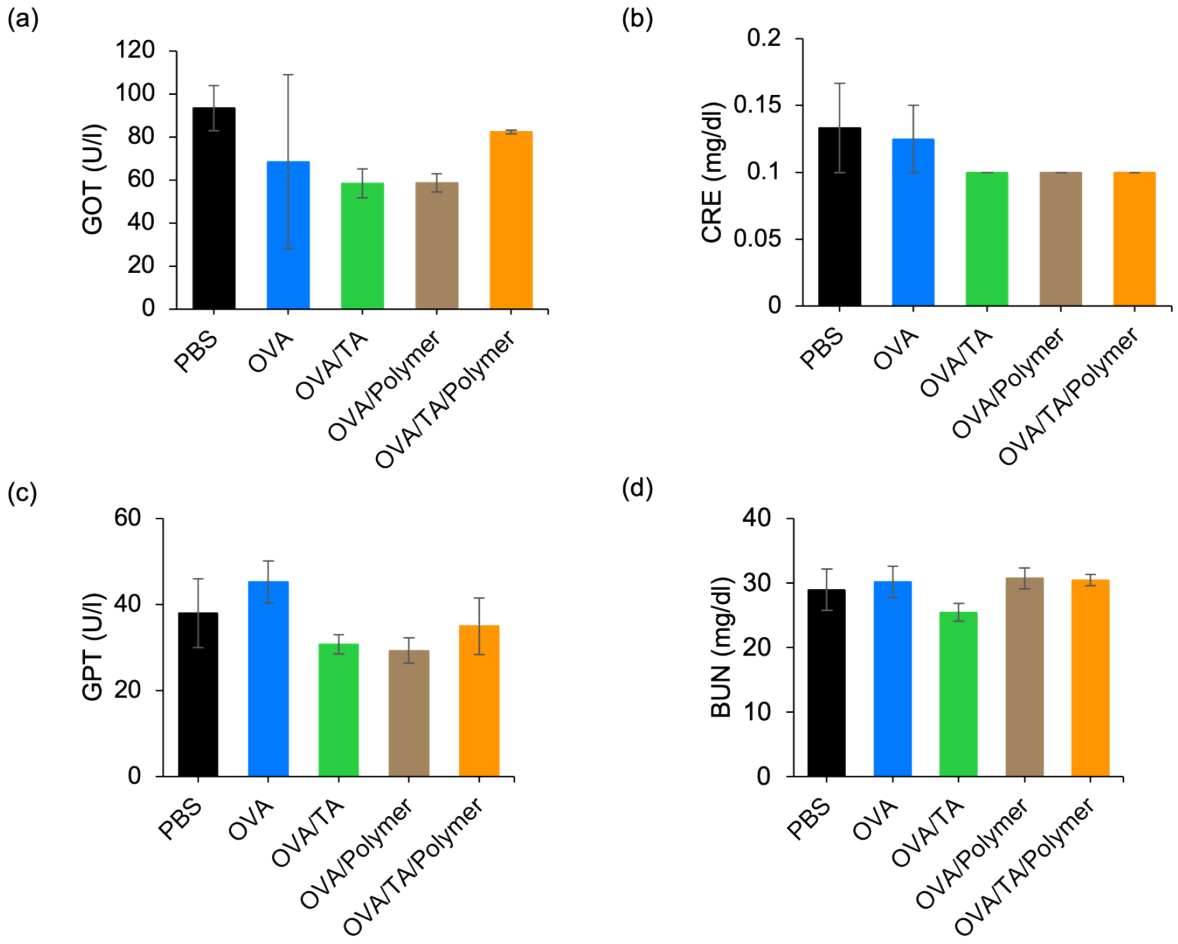

Figure S13. Blood parameters. Whole blood was collected 48 hours after s.c. injection of OVA samples (OVA: 10 μg per mouse; n = 4 mice). Biochemical parameters were evaluated, including (a) GOT, (b) CRE, (c) GPT and (d) BUN. GOT; glutamic oxaloacetic transaminase, CRE; creatinine, GPT; glutamic pyruvic transaminase, BUN; blood urea nitrogen. The results are expressed as mean ± SEM.

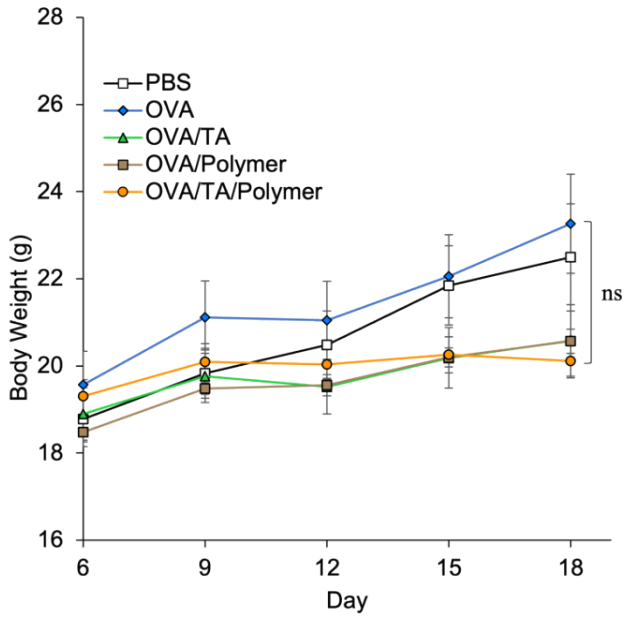

Figure S14. Body weight monitoring in the E.G7-OVA prophylactic model. OVA samples were injected s.c. on days 0 and 7, followed by an E.G7-OVA tumor challenge on day 14. Body weight was monitored over time (OVA: 10 μg per mouse; n = 5 mice). The results are expressed as mean ± SEM. Statistical significance was determined by ANOVA with Tukey's multiple comparison test.

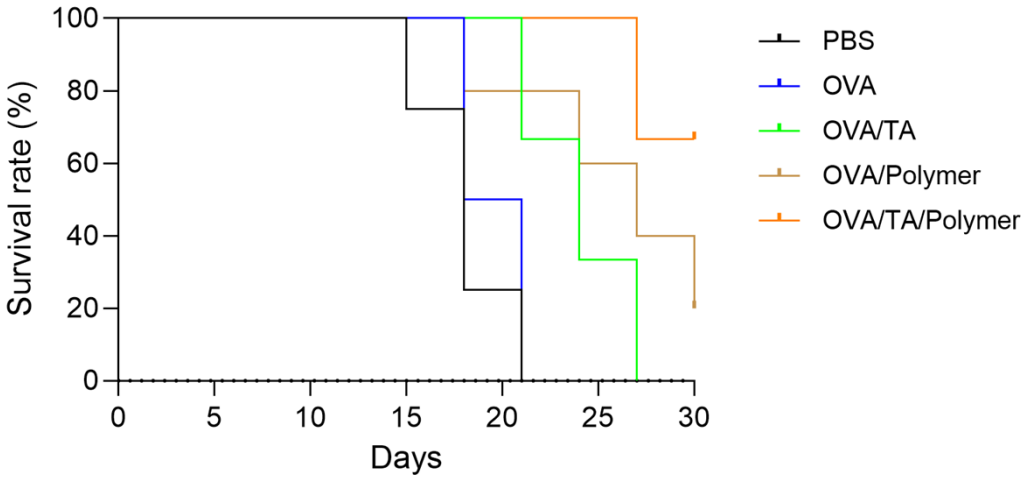

Figure S15. Kaplan-Meier survival curves of the E.G7-OVA prophylactic model. Survival was determined as the time until tumor reached 3000 mm^3. Data were plotted and analyzed using GraphPad Prism 10.0.

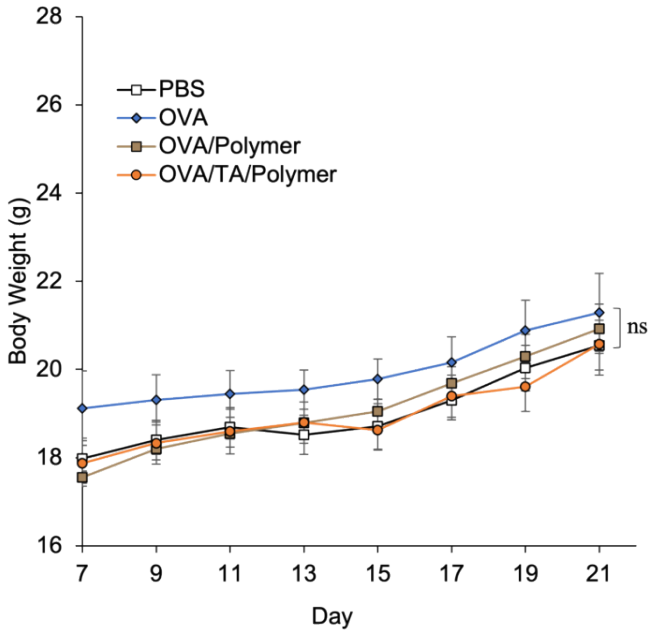

Figure S16. Body weight monitoring in the E.G7-OVA therapeutic model. Mice were inoculated with E.G7-OVA tumors on day 0 and injected s.c. with OVA samples on days 7, 11, 15 and 19. Body weight was monitored over time (OVA: 20 μg per mouse; n = 6 mice). The results are expressed as mean ± SEM. Statistical significance was determined by ANOVA with Tukey's multiple comparison test.

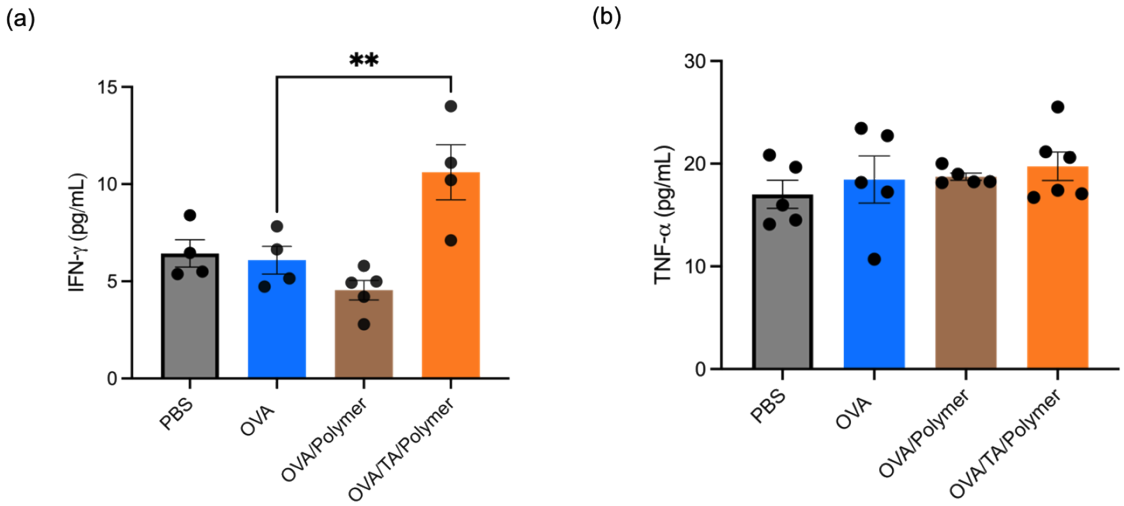

Figure S17. Cytokine expression in tumor tissue from the E.G7-OVA therapeutic model. Tumors were harvested and analyzed by ELISA for (a) IFN-γ and (b) TNF-α expression (OVA: 20 μg per mouse; n = 4 or 5 mice). Data are presented as mean ± SEM. Statistical significance was determined by ANOVA with Tukey's multiple comparison test.